ACS APPLIED MATERIALS & INTERFACES

Research Article

www.acsami.org

Simultaneous Nitrogen Doping and Pore Generation in Thermo-Insulating Graphene Films via Colloidal Templating

Hyunwoo Bark,[†] Jeongmin Lee,[†] Hosun Lim,[‡] Hye Young Koo,[§] Wonmok Lee,*[,∥] and Hyunjung Lee*[,†]

[†]School of Advanced Materials Engineering, Kookmin University, 77 Jeongneung-ro, Seongbuk-gu, Seoul 136-702, Republic of Korea

[‡]Electronic Materials & Device Research Center, Korea Electronics Technology Institute, 25 Saenariro, Bundanggu, Seongnamsi, Gyeonggido 463-816, Republic of Korea

[§]Korea Institute of Science and Technology, 92 Chudong-ro, Bongdong-eup, Wanju-gun, Jeollabuk-do 565-905, Republic of Korea

[∥]Department of Chemistry, Sejong University, 209 Neungdong-ro, Gwangjin-gu, Seoul 143-747, Republic of Korea

Supporting Information

ABSTRACT: We report a simple method for preparing highly efficient thermoelectric materials through the fabrication of nitrogen-doped reduced graphene oxide (GO) with a porous structure. The samples were produced by thermal annealing of GO/nitrogen-rich polystyrene (N-PS) particle composite films using a colloidal templating method. N-PS particles served as a nitrogen dopant source for the nitrogen-doped thermally reduced graphene oxide (TrGO) as well as sacrificial particles for the porous structure. The *S* values of the porous TrGO films were negative, indicating that the samples were transformed into n-type materials. Their porous structures simultaneously resulted in materials with high σ values and low in-plane κ values by providing numerous air cavities for phonon scattering and destruction of the anisotropic structure, maintaining an interconnected structure for an electron transport path. Thus, the porous TrGO films exhibited enhanced power factors and low κ values. The highest ZT value of 1.39×10^{-4} was attained for a porous TrGO film annealed at 1100 °C, which was 1200 times higher than that of a nonporous TrGO film. This study emphasizes that an isotropic orientation of two-dimensional materials has a significant effect on the suppression of in-plane κ, leading to their enhanced thermoelectric performance.

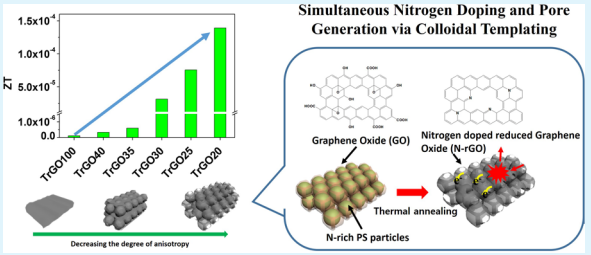

KEYWORDS: *ZT, reduced graphene oxide, nitrogen doping, colloidal templating, porous structure*

INTRODUCTION

Because power generation using the combustion of fossil fuels or nuclear power plants causes serious environmental pollution problems, there has been a technological trend to seek eco-friendly power-generation sources. For instance, thermoelectric power generation has become an attractive candidate for many industrial applications. With the carrier transportation resulting from a temperature gradient, there are no moving parts in thermoelectric devices, and the resources for this technology surround us in forms such as waste heat and body temperature. For thermoelectric power to be a meaningful renewable energy resource, an n-type or p-type semiconductor material with a high figure of merit (ZT), which is representative of the material's performance, is needed. ZT is defined as $ZT = S^2\sigma T/\kappa$, where *S*, σ, κ, and *T* are the Seebeck coefficient, electrical conductivity, thermal conductivity, and absolute temperature, respectively. Highly efficient thermoelectric materials require a high σ, high *S*, and low κ. To date, state of the art thermoelectric materials usually consist of inorganic alloys based on Te applied in the low-temperature region (<400 °C).[1]

Recently, two issues have arisen regarding novel thermoelectric materials. The first issue concerns the severe limitations of inorganic materials such as their brittleness, high density, and high cost. To overcome these limits, nanocarbon materials (carbon nanotubes (CNTs) or graphene), conducting polymers, and their composites have been studied as alternative thermoelectric materials. Their organic nature enables their fabrication as durable and flexible films. Even though conducting polymers or their composites with nanocarbon exhibit high ZT values,[2,3] difficulties still arise in their application at high temperatures above 300 °C. To attain high thermal stability as flexible films, pure nanocarbon materials are preferred. For example, Yanagi et al. investigated the thermoelectric properties of semiconducting single-walled nanotubes upon modulating their energy levels.[4] Graphene and reduced graphene oxide (rGO) are also attractive thermoelectric materials because of their superior σ. Single-layer or few-layer graphene has been prepared by exfoliation from graphite using sticky tape or chemical vapor deposition. Their thermoelectric properties were studied by controlling the amount of charged carriers as a function of oxidation level, for example.[5,6] However, previous studies have focused on a

Received: August 7, 2016
Accepted: October 24, 2016
Published: October 24, 2016

DOI: 10.1021/acsami.6b09836
ACS Appl. Mater. Interfaces 2016, 8, 31617−31624

Scheme 1. Schematic Diagram of Fabrication of N-Doped Reduced Graphene Oxide Porous Structure

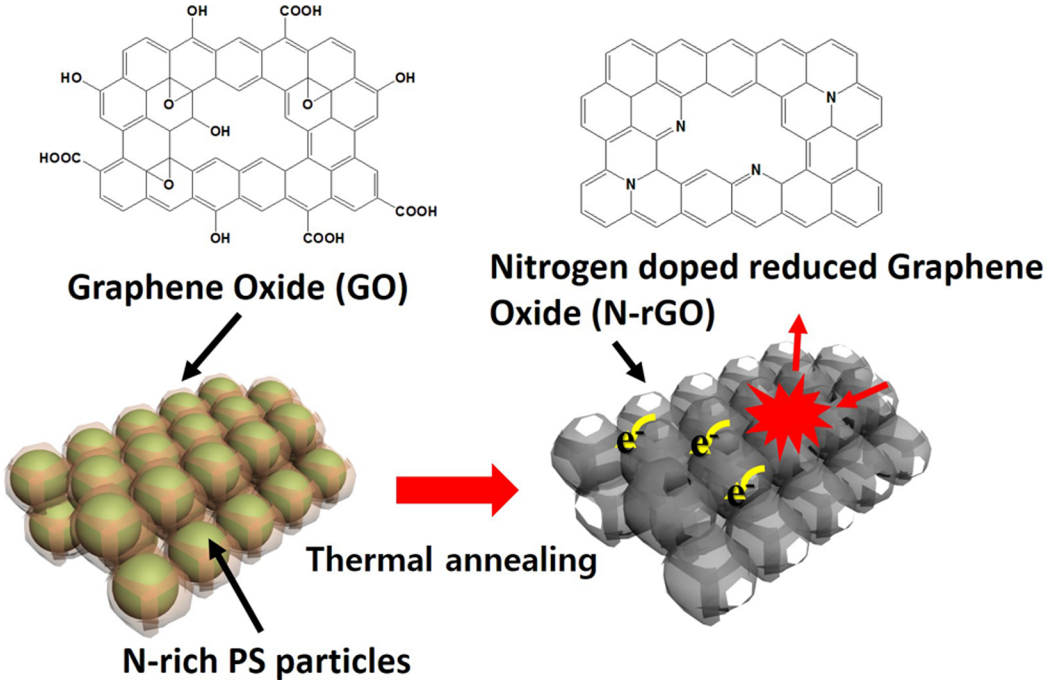

fundamental understanding of the energy diagram in graphene or reduced graphene oxide, and no information concerning their thermal conductivity has been provided.[7,8] To evaluate their overall thermoelectric performance, their thermal conductivities should also be considered. rGO contains numerous defects which originate during the harsh oxidation process; thus, there are abundant places for doping. The electrical properties of rGO can be readily controlled by doping rGO with impurities. Defects in the sp^2 hybridized electronic structures in rGO intrinsically induce p-type characters as thermoelectric materials. The preparation of n-type rGO remains challenging for thermoelectric materials. The encapsulation of nanocarbon with nitrogen-rich organic materials such as triphenylphosphine (TPP), polyethylenimine (PEI), and urea successfully converted nanocarbon into n-type materials,[9−12] but limitations of thermal stability have been entailed. A recent study reported the presence of thermally substituted nitrogen in rGO from gaseous ammonia, reaching a nitrogen doping level of approximately 3%.[13]

The second issue is that it is difficult to obtain low κ and high σ simultaneously. The total κ consists of the electronic thermal conductivity (κ_e) and lattice vibrational thermal conductivity (κ_L). High σ is associated with high κ_e because of the high carrier concentration. Therefore, the total κ can be reduced by suppressing κ_L while keeping σ high. Recent studies reported the effective reduction of κ_L by controlling grain boundaries or introducing porous structures.[14−18] At this point, we must consider anisotropic structures in a thin film structure of CNTs or graphene. The in-plane κ (*XY*-direction) of graphene is 2 orders of magnitude larger than that of the through-plane (*Z*-direction) because of sp^2 hybridization.[19−22] For example, the in-plane κ of single-layer graphene or rGO is known to be $\sim 10^3$ W/mK.[23,24] When a few micrometer-thick CNT or graphene film is used in a thermoelectric device, a temperature gradient is effectively generated along the in-plane direction, while thermal equilibrium is rapidly attained along the thickness direction. Therefore, low in-plane κ is required to achieve a high-performance thermoelectric property. However, most recent studies have used the through-plane κ in considering the thermoelectric properties with σ being measured in-plane. Attention must be paid to avoid misinterpreting the final performance of a thermoelectric device based on these contradictory characterizations. Recently, Zhou et al. reported a thermoelectric performance of carbon nanotubes with measuring in-plane thermal conductivity.[25]

In this study, we synthesized nitrogen-rich polystyrene (N-PS) particles using emulsion polymerization and fabricated porous structures of thermally reduced graphene oxide (TrGO) using simultaneous nitrogen doping. The samples were produced by thermal annealing of GO/PS particle composite films prepared using a colloidal templating method.[26,27] To study the effect of nitrogen doping and porous structures on the thermoelectric properties of TrGO, porous structures of TrGO with different porosities were produced by increasing the PS particle content with a fixed amount of TrGO. The PS particles served as both sacrificial particles for the porous structure and a nitrogen dopant source for the nitrogen-doped TrGO. The volume percent of TrGO is indicated after TrGO in the sample codes. Upon increasing the film porosity, we observed that σ of the samples increased, whereas *S* became negative (i.e., n-type materials) because of the nitrogen doping. In addition, the in-plane κ decreased significantly because of the higher porosity. For the porous structures, we compared the in-plane and through-plane κ values. The orientation of paper-like two-dimensional TrGO could be tuned either in parallel to or out of the substrate in a porous film because of the PS particles. For comparison, we prepared nonporous films in which most of the TrGO plates were parallel to the substrate; the films exhibited anisotropic properties. We demonstrated that the randomly laid TrGOs could lead to a remarkable reduction in the in-plane κ while maintaining similar σ. Thus, the power factor and ZT value were enhanced. An important advantage of this method is that nitrogen doping and pore generation occur

DOI: 10.1021/acsami.6b09836
ACS Appl. Mater. Interfaces 2016, 8, 31617−31624

simultaneously during thermal annealing of GO/PS particle composite films.

RESULTS AND DISCUSSION

To achieve simultaneous nitrogen doping and pore generation, N-PS particles were synthesized using polyvinylpyrollidone (PVP) as a surfactant and 2,2′-azobis(2-methypropionamide) dihydrochloride (AIBA) as an initiator during emulsion polymerization. We calculated the diameter of the synthesized PS particles (approximately 260 nm) using the maximum wavelength in the optical reflectance spectrum and the modified Bragg equation[28] (Figure S1). The ζ-potential of the PS particles was 32 ± 3 mV because of the presence of nitrogen-containing PVP and AIBA on the surface of the PS particles. The PVP and AIBA also induced good dispersion among the negatively charged GO sheets. When the GO/PS composite film was fabricated, the amount of GO was fixed, and the amount of PS was increased to control the porosity in each film. After thermal annealing, pores were observed in the composite films, which indicates that PS was removed, as illustrated in Scheme 1.

Figure 1 presents SEM images showing the morphologies of the GO, TrGO, and porous TrGO films treated at 1100 °C.

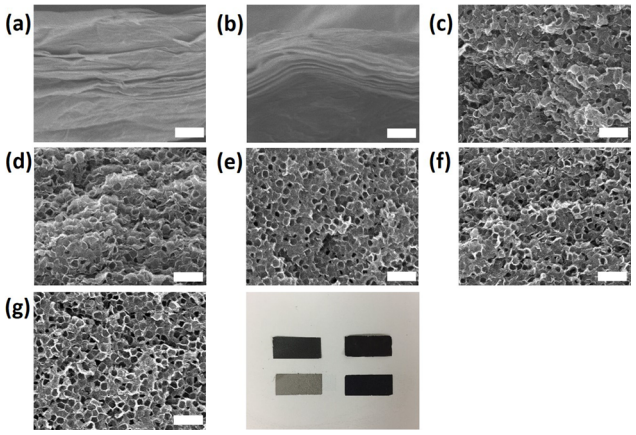

Figure 1. Cross-sectional SEM images of GO and PS composite annealed at 1100 °C and optical image of samples (a) GO, (b) TrGO100, (c) TrGO40, (d) TrGO35, (e) TrGO30, (f) TrGO25, and (g) TrGO20, and optical images of GO (left top), TrGO (left bottom), PS70 (right top), and TrGO30 (right bottom) films. All scale bars indicate 1 μm.

Without PS particles, the GO and TrGO100 films exhibited parallel-laid structures because of the two-dimensional structures of GO. The orientation of TrGO became much more isotropic upon increasing the PS particle content because of the pores generated after thermal annealing. In addition, increasing the PS content resulted in an increased number of pores with larger pore density because of the closer packing of sacrificial PS particles. In addition, the thickness of the films was observed to increase upon increasing the PS content at a fixed amount of GO. The film thicknesses were measured to be 8, 14, 15, 16, 17, and 18 μm for TrGO100, TrGO40, TrGO35, TrGO30, TrGO25, and TrGO20, respectively. The complete decomposition of PS was confirmed by thermogravimetric analysis (Figure S-2). In Figure 1 (optical image), the TrGO30 film is black, whereas the TrGO100 film is gray, indicating that the porous films absorb light even though TrGO100 scatters some light because of the parallel laid structures.

XPS analysis was used to characterize the atomic contents of the GO, TrGO100, and porous TrGO films as well as their chemical bonding states and temperature dependence. The atom % was calculated based on the peak areas corresponding to each atom in the XPS data. The oxygen contents were approximately 30% for GO and were reduced to less than 6% after thermal annealing. The oxygen contents decreased slightly at higher temperatures while showing no dependence on the porosity, i.e., the amount of sacrificed PS particles (Figure S3). The morphologies of the porous TrGO films treated thermally at 800 and 1000 °C are displayed in Figures S4 and S5, respectively.

Figure 2 presents XPS spectra of C 1s obtained from the GO and TrGO films (TrGO100) after thermal annealing at 800,

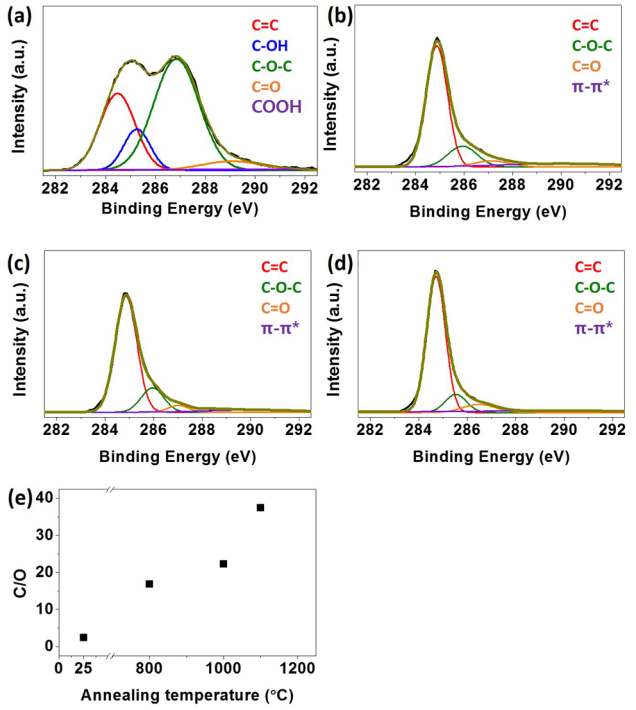

Figure 2. Carbon 1s XPS data acquired for (a) graphene oxide (GO) film and (b–d) TrGO100 films annealed at different annealing temperatures (b) 800 °C, (c) 1000 °C, (d) 1100 °C, and (e) C/O ratio values as a function of annealing temperature, respectively.

1000, and 1100 °C under Ar atmosphere. The two main peaks in GO in Figure 3a correspond to C═C bonding and oxygen-bonded carbons, respectively. Specifically, C═C, C−OH, C−O−C, C═O, and COOH peaks were detected at 284.5, 285.3, 286.7, 289.0, and 290.4 eV, respectively. Diverse oxygen-bonded carbon peaks were produced by the oxidative reactions

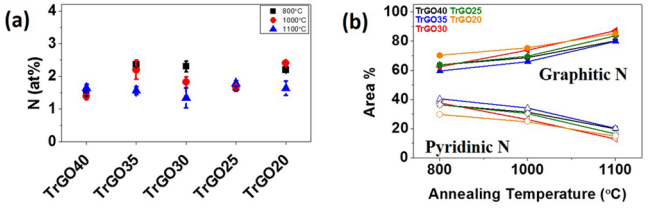

Figure 3. (a) Variation of nitrogen atom contents and (b) variation of graphitic N and pyridinic N peaks in porous TrGO films at different annealing temperatures.

DOI: 10.1021/acsami.6b09836
ACS Appl. Mater. Interfaces 2016, 8, 31617−31624

that occur when Hummer's method is applied. After thermal annealing of GO, the intensity of the oxygen-containing functional groups was significantly reduced, whereas the intensity of C═C bonding (~284.8 eV) increased remarkably, which is good agreement with literature reports.[29,30] The ratio of C/O was calculated from C and O atomic percentages in XPS spectra and was increased up to 40 at 1100 °C. This finding supports the effective thermal reduction of the GO films. Thermal treatment at higher temperatures produced a similar or slightly higher content of C═C in the TrGO100 films, which indicates that a higher-temperature treatment increases the sp^2 characters and achieves the graphitic structure. The porous TrGO films exhibited a similar tendency, and their XPS spectra are presented in Figure S6.

Although TrGO100 did not exhibit a N 1s peak, the weak existence of a nitrogen peak was detected in porous TrGO films prepared with N-PS particles, and the content of doped nitrogen remained approximately 2% regardless of the porosity and annealing temperature (Figure 3a). In a recent study, nitrogen atoms were doped in GO at 3−5 atom % under a continuous flow of ammonia/Ar gas.[13] The limited dopant source of our nitrogen-containing PS particles resulted in slightly lower nitrogen doping compared with the value reported in the literature. However, our doping process was accompanied by the fabrication of a porous structure, which is effective in producing high-performance thermoelectric materials. In the remaining part of this study, the porous TrGO films will be referred to as N-doped TrGO based on XPS analysis. High-resolution XPS spectra of N 1s were investigated to determine the bonding configuration of the nitrogen atoms in TrGO20 as a function of the annealing temperature (Figure 4).

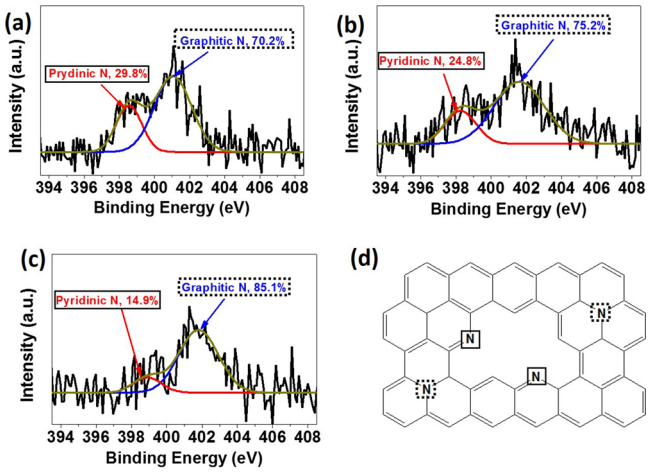

Figure 4. Nitrogen 1s XPS data acquired for graphene oxide films (TrGO20) annealed at different reduction temperatures as noted above the spectra: (a) 800, (b) 1000, and (c) 1100 °C. (d) Schematic diagram of nitrogen-doped reduced graphene oxide.

The N 1s spectra in Figure 4 reveal two characteristic peaks of pyridinic and graphitic nitrogen. The binding energies of the pyridinic and graphitic nitrogen were located at 398.3−398.9 and 401.0−401.8 eV, respectively. At a higher annealing temperature, the area of graphitic nitrogen increased from 70.2 to 85.1%, whereas that of pyridinic nitrogen decreased from 29.8 to 14.9% (Figure 3b). Because the graphitic nitrogen does not indicate nitrogen addition in edge or defect sites in TrGO but indicates replacement of carbon with nitrogen atoms in sp^2 hybridized structures, an increase in graphitic nitrogen implies the enhancement of the conjugated length in graphene materials, i.e., an effective structure for electron transport in n-type materials.[31] In addition, graphitic N-doped graphene provides a work function lower than that of pyridinic N-doped graphene, and the Fermi level is shifted upward in the band diagram, resulting in an effective nitrogen-doping effect.[32,33] For further analysis of the thermoelectric properties, TrGO films annealed at 1100 °C were used because their higher portion of graphitic N was expected to contribute an enhanced n-doping effect.

To compare the thermoelectric properties of the nonporous TrGO100 and porous and N-doped TrGO films, their σ, S, and κ values were investigated. Figures 5a and b display σ and S of

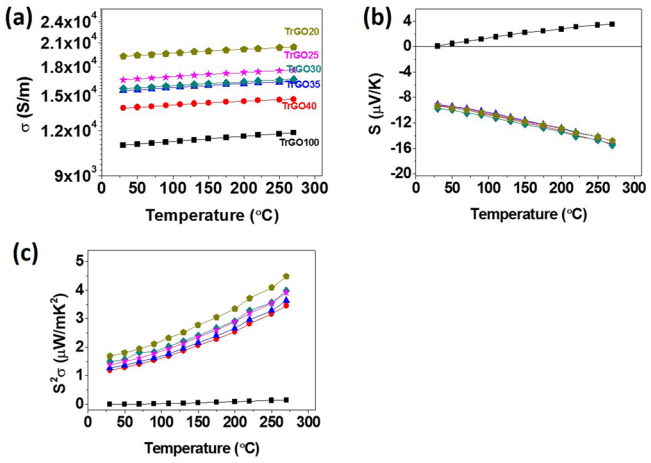

Figure 5. Temperature dependence of (a) electrical conductivity, (b) Seebeck coefficient, and (c) power factor for thermally reduced graphene oxide films annealed at 1100 °C.

TrGO100 and porous TrGO measured at ambient temperature. The temperature-dependent σ measurement of every TrGO film had a positive slope, which implies that the films exhibited semiconductor characteristics. The σ values of the porous TrGO films were higher than those of TrGO100 in the entire temperature range (30−270 °C). In detail, σ of TrGO100 remained approximately 11000−12000 S/m, which was lower than that of porous TrGO (>13000 S/m). A maximum σ of 20500 S/m was achieved at 270 °C for TrGO20, which was nearly twice the value of TrGO100. Increased σ values in N-doped TrGO can be explained by the graphitic nitrogen doping in TrGO. As expressed in the XPS analysis, the graphitic nitrogen that replaced carbon atoms in TrGO can donate electrons, resulting in an increased electron concentration. Broadly delocalized electrons arising from graphitic nitrogen through sp^2 hybridization can enhance electron transport, resulting in improved electrical properties.[34] An interesting point is that σ was increased upon increasing the porosity from TrGO40 to TrGO20. With higher porosity, the percolation between rGO sheets increased, resulting in a high σ.[35,36] Although there was no significant difference in the nitrogen atomic percentages in all the porous TrGO films, their three-dimensional interconnected network structures provide more effective transport paths for electrons. Moreover, nitrogen doping on the TrGO surface increased the electrical conductivity. Even though the mobility of the samples was decreased slightly as a function of porosity, the increase in

DOI: 10.1021/acsami.6b09836
ACS Appl. Mater. Interfaces 2016, 8, 31617−31624

carrier concentration provided higher electrical conductivity. (Figure S7)

The measured S of TrGO100 was approximately 0.1 μV/K at 30 °C, which indicates that there was almost no thermoelectric potential generated by the temperature gradient (Figure 5b). Such a low S value indicates that electrons and holes in TrGO100 diffuse at the same rate in the presence of a temperature gradient, canceling out the electrical potential.[5] However, the S values of the N-doped TrGOs were in the range of −9.1 to −9.8 μV/K for the same temperature gradient. The inversion of the S sign from positive to negative value is further evidence of nitrogen doping on TrGO resulting from the abundant electrons as dominant charge carriers.

The absolute value of S of all the samples increased as a function of temperature (30−270 °C). The temperature dependence of S is related to the movement of charge carriers in the samples. For TrGO100, S was approximately 0.1 μV/K at 30 °C, which implies that the charge carriers of the sample were slightly dominated by holes. At 270 °C, S increased to 3.5 μV/K, which indicates that holes were more dominant at 270 °C than at 30 °C. In other words, the p-type character of TrGO100 was observed to be stronger at a higher temperature. However, the S values of N-doped TrGO20 decreased from −9.4 to −14.8 μV/K because of the high abundance of electrons after nitrogen doping. The temperature dependence of the S values of the other TrGO films showed a tendency similar to that of TrGO20 with no dependence on the PS content. With the obtained σ and S, the power factor ($S^2\sigma$) was calculated to evaluate the thermoelectric properties of the sample without κ. The power factor increased in the N-doped TrGOs compared with that of TrGO100, and larger values were obtained at higher temperatures, reflecting the increased σ and S (Figure 5c). A maximum power factor of approximately 4.5 μW/mK^2 with TrGO20 at 270 °C was achieved. Despite the similar S values in N-doped TrGO for the entire temperature range, the power factor of TrGO20 was the highest because its σ was the highest.

κ was calculated by multiplying the density, specific heat, and thermal diffusivity, which were measured at 25 °C (Figure 6). At this point, we separately considered the in-plane and through-plane thermal diffusivity (α_{in} and α_{th}) because a temperature gradient is generated along the in-plane direction in TrGO thin films. We expect that the pores in porous TrGO films disturb the orientation of two-dimensional graphene as in the "paper piled structure" of the TrGO100 film. Figure 6 demonstrates several interesting behaviors of the in-plane and through-plane κ (κ_{in} and κ_{th}) values as a function of porosity. First, in TrGO100, the in-plane κ (~1284 W/mK) was 10^5 times larger than the through-plane κ (~0.01 W/mK) because of the paper-piled structure, resulting in a significantly large anisotropy in κ, as observed in Figure 2b (Figure 6a). In this work, κ_{in} of TrGO100 annealed at 1100 °C was slightly lower than the reported value (~5000 W/mK) in single-layer graphene,[23,37,38] which may originate from the phonon scattering at the interfaces of rGO flakes in TrGO100. However, κ_{in} of TrGO100 was higher than or similar to the reported value with annealed rGO film.[24,39−41] In detail, κ_{in} of rGO film was different depending on the sample preparation. With an increase in the amount void in the rGO film, κ_{in} was decreased. In the case of TrGO100 prepared in this study, the higher κ_{in} was suspected by higher packing state. The low κ_{th} arises from the many interfaces among the laid rGO sheets as thermal barriers. As observed in Figure S8, the thickness of an rGO sheet synthesized in this study was estimated to be under 1 nm by atomic force microscopy. The thickness of the TrGO100 film was approximately 8 μm; therefore, we presumed that more than ~8000 layers of GO were stacked in a film. Similarly, in a superlattice structure, it is well-known that the through-plane κ remains low because of phonon scattering at the interfaces.[42,43] In the porous TrGO films, the in-plane κ decreased as a function of porosity, whereas the through-plane κ increased slightly. Notably, the differences between the in-plane and through-plane κ values decreased with increasing porosity, and the values merged at a similar level. The κ_{in} and κ_{th} values of TrGO20 were approximately 3.6 and 0.9 W/mK, respectively. This asymptotic behavior of the κ values can be explained by the isotropic thermally conductive structure resulting from the pores in the TrGO films, which hinder the formation of the paper-piled structure of TrGO.

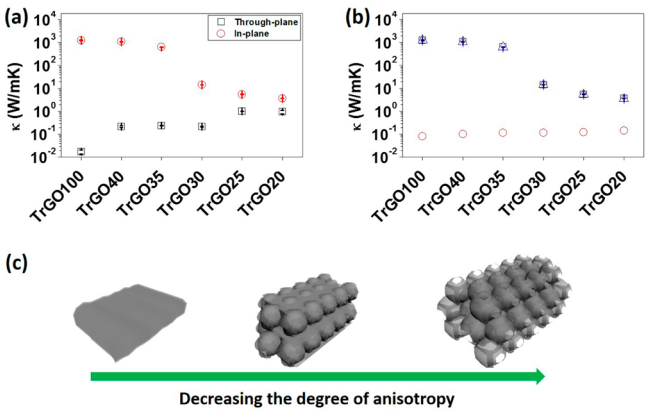

Figure 6. Porosity dependence of (a) in-plane and through-plane thermal conductivity and (b) electronic and lattice thermal conductivity in in-plane thermal conductivity for TrGO films annealed at 1100 °C. (c) Schematic diagram of porous reduced graphene oxide structure.

When we investigate the thermoelectric properties of a thin film sample, a temperature gradient is generated along the in-plane direction. Similar to how S and the electrical properties were measured along the in-plane direction, the κ_{in} should be considered instead of the κ_{th} to precisely understand the thermoelectric properties. The κ_{in} was separated from κ_e and κ_L. κ_e was calculated using the Wiedemann−Franz law, $\kappa_e = L\sigma T$, where L is the Lorenz number (2.45×10^{-8} V^2/K^2). κ_L was obtained by subtracting κ_e from κ_{in}. Figure 6b shows that the contribution of κ_e to κ in the TrGO samples was considerably low (~0.1 W/mK), and thus, the low κ arises mainly from a reduced κ_L. κ_e increases slightly for a large σ; however, κ_L rapidly decreases because of the destroyed paper-piled structure, where the pores in the TrGO films behave as a thermal insulator while increasing the chances for phonon scattering.

On the basis of $S^2\sigma$ and the in-plane κ, ZT was calculated (Figure 7). The ZT of TrGO100 annealed at 1100 °C was 1.15×10^{-7}, whereas that of TrGO20 annealed at 1100 °C was 1.39×10^{-4}, which is 1200 times higher. Because of the higher power factor and lower κ, ZT was significantly increased.

CONCLUSION

In conclusion, we provided a simple method for preparing highly efficient thermoelectric materials through the fabrication of N-doped rGO with a porous structure. Nitrogen doping

DOI: 10.1021/acsami.6b09836
ACS Appl. Mater. Interfaces 2016, 8, 31617−31624

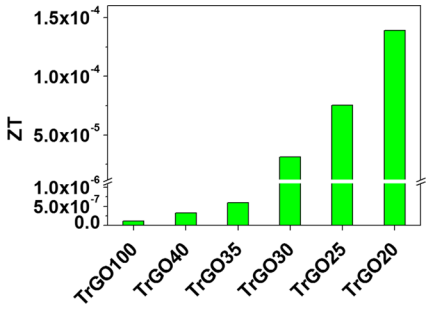

Figure 7. Porosity dependence of ZT values for TrGO films.

increased σ by increasing the electron density of the graphene materials. The porous structures simultaneously resulted in materials with high σ values and low in-plane κ values by providing numerous air cavities for phonon scattering and destruction of the anisotropic structure, maintaining an interconnected structure for an electron transport path. The S values of the porous TrGO films were negative, indicating that the samples were transformed into n-type materials. Thus, the porous TrGO films exhibited enhanced power factors and low κ values. A ZT value of 1.39×10^{-4} was attained for TrGO20 annealed at 1100 °C, which was 1200 times higher than that of TrGO100. Finally, N-doped TrGO films with porous structures were confirmed to simultaneously exhibit high σ and low κ. The colloidal templating method using other atom-rich polymeric particles could be used in simultaneous doping and pore generation, and following studies are in progress.

EXPERIMENTAL SECTION

Materials. To obtain GO, commercial graphite powder (SP-1, BAY CARBON Inc., United States) was used. $NaNO_3$ and $KMnO_4$ were purchased from Sigma-Aldrich. For synthesis of N-PS, PVP ($M_w \sim$ 40,000), AIBA as an initiator, styrene monomer, and aluminum oxide for purifying styrene monomer were purchased from Sigma-Aldrich. All chemicals were used as received.

Fabrication of Graphite Oxide and Graphene Oxide Solution. GO was prepared via Hummer's method from graphite powder.[44] Briefly, 1 g of graphite powder and 0.5 g of $NaNO_3$ were dissolved in H_2SO_4 (25 mL) with stirring for 1 h with the reaction flask kept in ice bath. Then, 3 g of $KMnO_4$ was added in the mixture with stirring for 1 h, and the temperature was increased gradually to 35 °C. H_2O (46 mL) was added to the mixture, followed by addition of a mixture of H_2O and H_2O_2 (140 and 2.5 mL, respectively). The resulting mixture was washed with 10% HCl solution and deionized water. Finally, the wet product was freeze-dried to obtain graphite oxide powders.

To prepare GO solution, 200 mg of graphite oxide powder was dispersed in 40 mL of H_2O in an ultrasonic bath for 1 h at room temperature. After dispersion, the solution was centrifuged at 3000 rpm for 5 min. Finally, the clear dark brown supernatant solution was obtained.

Synthesis of N-PS Particles. N-PS particles were synthesized by emulsion polymerization. After H_2O (26 mL) was degassed under nitrogen gas for an hour, 648 mg of PVP was dissolved in 3 mL of degassed H_2O, and 35 mg of AIBA as an initiator was dissolved in 1 mL of degassed H_2O. The styrene monomer (2.72 g), filtered through aluminum oxide for purification, was added in the solution dissolving PVP, and degassing was conducted for 30 min. The solution dissolving AIBA was injected rapidly, and the mixture was kept at 70 °C for 24 h. After the synthesis, the synthesized particle was poured in a dialysis tube (nominal MWCO 12000−14000), which was immersed in H_2O for another 3 days.

Fabrication of Nitrogen-Doped rGO Porous Structure. A measured amount of N-PS solution was dissolved in 20 mL of H_2O. GO solution was added in the solution and dispersed using an ultrasonic bath for 15 min at room temperature. The dispersion was filtered by a PTFE membrane (0.2 μm, Φ = 47 mm), and the filtered product was dried for 24 h at ambient conditions. After being removed from the membrane, the product was thermally annealed under Ar gas. To remove the PS completely, two step annealing was conducted. First, the temperature was increased from room temperature to 500 °C with a heating rate of 5 °C/min and remained for 1 h. Then, the temperature was increased to 1100 °C with the same rate and remained at 1100 °C for 2 h.

Characterization. For morphological properties, a TrGO film was characterized by field-emission scanning electron microscopy (FE-SEM, JSM-7401F, JEOL, Ltd.). To characterize the chemical bonding and atomic ratio of a TrGO film, X-ray photoelectron spectrometry (Kα, Thermo Scientific) was used, where mono anode Al Kα was used as the X-ray source. To measure σ, the four-point probe method was exploited. We used the current source meter (Keithley 2400) and obtained a sheet resistance from current−voltage measurement. The sheet resistance was converted into σ with a dimensional factor. S was obtained under a temperature gradient (ΔT) on a film. The potential difference (ΔV) was detected by nanovolt meter (Agilent 34420A). Four spots of voltages were pointed out with temperature gradient (ΔT), and linear fit was conducted. The linear correlation coefficient for S was greater than 0.99. σ and S were measured over a temperature range of room temperature to 270 °C. To confirm the reliability of the instrument, we surveyed σ and S of Ni (99.99%). The measured σ and S of Ni were 6.9×10^{-8} Ω·m and −21.5 μV/K, respectively. These data showed good accordance with a literature report.[45] Multiplication of σ and S^2 gives a power factor ($S^2\sigma$). Thermal conductivity (κ) was determined by multiplying density (D), specific heat (C_p), and thermal diffusivity (α) (Figure S9). First, D was calculated by mass (m)/volume (V) of the sample. To have in-plane and through-plane thermal conductivity (κ_{in} and κ_{th}), in-plane direction and through-plane direction of thermal diffusivity (α_{in} and α_{th}) were measured. α was obtained by the laser flash method (LFA 457, NETZSCH). α_{in} was obtained with designed holder, illustrated in Figure S10. After application of the heat source in the sample, the heat was transported about 5 mm on in-plane direction of the sample. The heat travel distance was larger than the thickness of the samples (sample thickness: 10^0, $\sim 10^1$ μm; heat transport distance: ~5 mm). The method for obtaining α_{in} is similar to reported literature.[39] The specific heat of samples was measured by differential scanning calorimetry (DSC214 Polyma, NETZSCH) with a graphite reference. The specific heat of graphite was 0.68 J/gK at 25 °C.

ASSOCIATED CONTENT

Supporting Information

The Supporting Information is available free of charge on the ACS Publications website at DOI: 10.1021/acsami.6b09836.

Additional figures and experimental details (PDF)

AUTHOR INFORMATION

Corresponding Authors

*E-mail: wonmoklee@sejong.ac.kr.
*E-mail: hyunjung@kookmin.ac.kr.

Notes

The authors declare no competing financial interest.

ACKNOWLEDGMENTS

H.L. acknowledges financial support for this work given by the National Research Foundation of Korea Grant funded by the Korean Government (Grants NRF-2014R1A1A3052933 and 2015R1A5A7037615) and the Civil Military Technology Cooperation Center (Grant 15-CM-SS-03 and 15-CM-EN-08).

DOI: 10.1021/acsami.6b09836
ACS Appl. Mater. Interfaces 2016, 8, 31617−31624

REFERENCES

(1) Snyder, G. J.; Toberer, E. S. Complex Thermoelectric Materials. *Nat. Mater.* **2008**, *7* (2), 105−114.

(2) Bubnova, O.; Khan, Z. U.; Malti, A.; Braun, S.; Fahlman, M.; Berggren, M.; Crispin, X. Optimization of the Thermoelectric Figure of Merit in the Conducting Polymer poly(3,4-ethylenedioxythiophene). *Nat. Mater.* **2011**, *10* (6), 429−433.

(3) Wang, H.; Yi, S.-i.; Pu, X.; Yu, C. Simultaneously Improving Electrical Conductivity and Thermopower of Polyaniline Composites by Utilizing Carbon Nanotubes as High Mobility Conduits. *ACS Appl. Mater. Interfaces* **2015**, *7* (18), 9589−9597.

(4) Yanagi, K.; Kanda, S.; Oshima, Y.; Kitamura, Y.; Kawai, H.; Yamamoto, T.; Takenobu, T.; Nakai, Y.; Maniwa, Y. Tuning of the Thermoelectric Properties of One-Dimensional Material Networks by Electric Double Layer Techniques Using Ionic Liquids. *Nano Lett.* **2014**, *14* (11), 6437−6442.

(5) Zuev, Y. M.; Chang, W.; Kim, P. Thermoelectric and Magnetothermoelectric Transport Measurements of Graphene. *Phys. Rev. Lett.* **2009**, *102* (9), 096807.

(6) Cho, S.; Kang, S. D.; Kim, W.; Lee, E.-S.; Woo, S.-J.; Kong, K.-J.; Kim, I.; Kim, H.-D.; Zhang, T.; Stroscio, J. A.; Kim, Y.-H.; Lyeo, H.-K. Thermoelectric Imaging of Structural Disorder in Epitaxial Graphene. *Nat. Mater.* **2013**, *12* (10), 913−918.

(7) Xiao, N.; Dong, X.; Song, L.; Liu, D.; Tay, Y.; Wu, S.; Li, L.-J.; Zhao, Y.; Yu, T.; Zhang, H.; Huang, W.; Hng, H. H.; Ajayan, P. M.; Yan, Q. Enhanced Thermopower of Graphene Films with Oxygen Plasma Treatment. *ACS Nano* **2011**, *5* (4), 2749−2755.

(8) Choi, J.; Tu, N. K.; Lee, S.-S.; Lee, H.; Kim, J.; Kim, H. Controlled Oxidation Level of Reduced Graphene Oxides and its Effect on Thermoelectric Properties. *Macromol. Res.* **2014**, *22* (10), 1104−1108.

(9) Yu, C.; Murali, A.; Choi, K.; Ryu, Y. Air-stable Fabric Thermoelectric Modules Made of N- and P-type Carbon Nanotubes. *Energy Environ. Sci.* **2012**, *5* (11), 9481−9486.

(10) Nonoguchi, Y.; Ohashi, K.; Kanazawa, R.; Ashiba, K.; Hata, K.; Nakagawa, T.; Adachi, C.; Tanase, T.; Kawai, T. Systematic Conversion of Single Walled Carbon Nanotubes into n-type Thermoelectric Materials by Molecular Dopants. *Sci. Rep.* **2013**, *3*, 3344.

(11) Ryu, Y.; Freeman, D.; Yu, C. High Electrical Conductivity and n-type Thermopower from Double-/Single-wall Carbon Nanotubes by Manipulating Charge Interactions between Nanotubes and Organic/Inorganic Nanomaterials. *Carbon* **2011**, *49* (14), 4745−4751.

(12) Bark, H.; Lee, W.; Lee, H. Enhanced Thermoelectric Performance of CNT Thin Film p/n Junctions Doped with N-containing Organic Molecules. *Macromol. Res.* **2015**, *23* (9), 795−801.

(13) Li, X.; Wang, H.; Robinson, J. T.; Sanchez, H.; Diankov, G.; Dai, H. Simultaneous Nitrogen Doping and Reduction of Graphene Oxide. *J. Am. Chem. Soc.* **2009**, *131* (43), 15939−15944.

(14) Li, J.-F.; Liu, W.-S.; Zhao, L.-D.; Zhou, M. High-performance Nanostructured Thermoelectric Materials. *NPG Asia Mater.* **2010**, *2*, 152−158.

(15) Dresselhaus, M. S.; Chen, G.; Tang, M. Y.; Yang, R. G.; Lee, H.; Wang, D. Z.; Ren, Z. F.; Fleurial, J. P.; Gogna, P. New Directions for Low-Dimensional Thermoelectric Materials. *Adv. Mater.* **2007**, *19* (8), 1043−1053.

(16) Han, Y.; Li, C.; Bian, C.; Li, S.; Wang, C.-A. Porous Anorthite Ceramics with Ultra-Low Thermal Conductivity. *J. Eur. Ceram. Soc.* **2013**, *33* (13−14), 2573−2578.

(17) Lo, Y. W.; Wei, W. C. J.; Hsueh, C. H. Low Thermal Conductivity of Porous Al_2O_3 Foams for SOFC Insulation. *Mater. Chem. Phys.* **2011**, *129* (1−2), 326−330.

(18) Chen, J.; Gui, X.; Wang, Z.; Li, Z.; Xiang, R.; Wang, K.; Wu, D.; Xia, X.; Zhou, Y.; Wang, Q.; Tang, Z.; Chen, L. Superlow Thermal Conductivity 3D Carbon Nanotube Network for Thermoelectric Applications. *ACS Appl. Mater. Interfaces* **2012**, *4* (1), 81−86.

(19) Choi, B. G.; Yang, M.; Hong, W. H.; Choi, J. W.; Huh, Y. S. 3D Macroporous Graphene Frameworks for Supercapacitors with High Energy and Power Densities. *ACS Nano* **2012**, *6* (5), 4020−4028.

(20) Kang, B.; Lim, S.; Lee, W. H.; Jo, S. B.; Cho, K. Work-Function-Tuned Reduced Graphene Oxide via Direct Surface Functionalization as Source/Drain Electrodes in Bottom-Contact Organic Transistors. *Adv. Mater.* **2013**, *25* (41), 5856−5862.

(21) Kim, T.; Kim, H.; Kwon, S. W.; Kim, Y.; Park, W. K.; Yoon, D. H.; Jang, A. R.; Shin, H. S.; Suh, K. S.; Yang, W. S. Large-Scale Graphene Micropatterns via Self-Assembly-Mediated Process for Flexible Device Application. *Nano Lett.* **2012**, *12* (2), 743−748.

(22) Liu, X.; Kim, H.; Guo, L. J. Optimization of Thermally Reduced Graphene Oxide for an Efficient Hole Transport Layer in Polymer Solar Cells. *Org. Electron.* **2013**, *14* (2), 591−598.

(23) Balandin, A. A. Thermal Properties of Graphene and Nanostructured Carbon Materials. *Nat. Mater.* **2011**, *10* (8), 569−581.

(24) Song, N.-J.; Chen, C.-M.; Lu, C.; Liu, Z.; Kong, Q.-Q.; Cai, R. Thermally Reduced Graphene Oxide Films as Flexible Lateral Heat Spreaders. *J. Mater. Chem. A* **2014**, *2* (39), 16563−16568.

(25) Zhou, W.; Fan, Q.; Zhang, Q.; Li, K.; Cai, L.; Gu, X.; Yang, F.; Zhang, N.; Xiao, Z.; Chen, H.; Xiao, S.; Wang, Y.; Liu, H.; Zhou, W.; Xie, S. Ultrahigh-Power-Factor Carbon Nanotubes and an Ingenious Strategy for Thermoelectric Performance Evaluation. *Small* **2016**, *12* (25), 3407−3414.

(26) Kwak, E. S.; Lee, W.; Park, N.-G.; Kim, J.; Lee, H. Compact Inverse-Opal Electrode Using Non-Aggregated TiO_2 Nanoparticles for Dye-Sensitized Solar Cells. *Adv. Funct. Mater.* **2009**, *19* (7), 1093−1099.

(27) Yang, S. C.; Yang, D. J.; Kim, J.; Hong, J. M.; Kim, H. G.; Kim, I. D.; Lee, H. Hollow TiO_2 Hemispheres Obtained by Colloidal Templating for Application in Dye-Sensitized Solar Cells. *Adv. Mater.* **2008**, *20* (5), 1059−1064.

(28) Kim, S.-G.; Seo, Y.-G.; Cho, Y.-J.; Shin, J.-S.; Gil, S.-C.; Lee, W.-M. Optimization of Emulsion Polymerization for Submicron-Sized Polymer Colloids Towards Tunable Synthetic Opals. *Bull. Korean Chem. Soc.* **2010**, *31* (7), 1891−1896.

(29) Zhou, G.; Paek, E.; Hwang, G. S.; Manthiram, A. Long-life Li/polysulphide Batteries with High Sulphur Loading Enabled by Lightweight Three-dimensional nitrogen/Sulphur-codoped Graphene Sponge. *Nat. Commun.* **2015**, *6*, 7760.

(30) Ganguly, A.; Sharma, S.; Papakonstantinou, P.; Hamilton, J. Probing the Thermal Deoxygenation of Graphene Oxide Using High-Resolution In Situ X-ray-Based Spectroscopies. *J. Phys. Chem. C* **2011**, *115* (34), 17009−17019.

(31) Hwang, J. O.; Park, J. S.; Choi, D. S.; Kim, J. Y.; Lee, S. H.; Lee, K. E.; Kim, Y.-H.; Song, M. H.; Yoo, S.; Kim, S. O. Workfunction-Tunable, N-Doped Reduced Graphene Transparent Electrodes for High-Performance Polymer Light-Emitting Diodes. *ACS Nano* **2012**, *6* (1), 159−167.

(32) Schiros, T.; Nordlund, D.; Pálová, L.; Prezzi, D.; Zhao, L.; Kim, K. S.; Wurstbauer, U.; Gutiérrez, C.; Delongchamp, D.; Jaye, C.; Fischer, D.; Ogasawara, H.; Pettersson, L. G. M.; Reichman, D. R.; Kim, P.; Hybertsen, M. S.; Pasupathy, A. N. Connecting Dopant Bond Type with Electronic Structure in N-Doped Graphene. *Nano Lett.* **2012**, *12* (8), 4025−4031.

(33) Lee, D. H.; Lee, W. J.; Lee, W. J.; Kim, S. O.; Kim, Y. H. Theory, Synthesis, and Oxygen Reduction Catalysis of Fe-Porphyrin-Like Carbon Nanotube. *Phys. Rev. Lett.* **2011**, *106* (17), 4.

(34) Wei, D.; Liu, Y.; Wang, Y.; Zhang, H.; Huang, L.; Yu, G. Synthesis of N-Doped Graphene by Chemical Vapor Deposition and Its Electrical Properties. *Nano Lett.* **2009**, *9* (5), 1752−1758.

(35) Cao, X.; Yin, Z.; Zhang, H. Three-dimensional Graphene Materials: Preparation, Structures and Application in Supercapacitors. *Energy Environ. Sci.* **2014**, *7* (6), 1850−1865.

(36) Dinh, D. A.; Hui, K. N.; Hui, K. S. Three Dimensional Graphene: A Prospective Architecture for High Performance Supercapacitors. *Energy Environ. Focus* **2014**, *3* (2), 98−120.

(37) Balandin, A. A.; Ghosh, S.; Bao, W.; Calizo, I.; Teweldebrhan, D.; Miao, F.; Lau, C. N. Superior Thermal Conductivity of Single-Layer Graphene. *Nano Lett.* **2008**, *8* (3), 902−907.

(38) Ghosh, S.; Calizo, I.; Teweldebrhan, D.; Pokatilov, E. P.; Nika, D. L.; Balandin, A. A.; Bao, W.; Miao, F.; Lau, C. N. Extremely High

DOI: 10.1021/acsami.6b09836
ACS Appl. Mater. Interfaces 2016, 8, 31617−31624

Thermal Conductivity of Graphene: Prospects for Thermal Management Applications in Nanoelectronic Circuits. *Appl. Phys. Lett.* **2008**, *92* (15), 3.
(39) Renteria, J. D.; Ramirez, S.; Malekpour, H.; Alonso, B.; Centeno, A.; Zurutuza, A.; Cocemasov, A. I.; Nika, D. L.; Balandin, A. A. Strongly Anisotropic Thermal Conductivity of Free-Standing Reduced Graphene Oxide Films Annealed at High Temperature. *Adv. Funct. Mater.* **2015**, *25* (29), 4664−4672.
(40) Kumar, P.; Shahzad, F.; Yu, S.; Hong, S. M.; Kim, Y.-H.; Koo, C. M. Large-area Reduced Graphene Oxide Thin Film with Excellent Thermal Conductivity and Electromagnetic Interference Shielding Effectiveness. *Carbon* **2015**, *94*, 494−500.
(41) Xin, G.; Sun, H.; Hu, T.; Fard, H. R.; Sun, X.; Koratkar, N.; Borca-Tasciuc, T.; Lian, J. Large-Area Freestanding Graphene Paper for Superior Thermal Management. *Adv. Mater.* **2014**, *26* (26), 4521−4526.
(42) Hicks, L. D.; Dresselhaus, M. S. Effect of Quantum-well Structures on the Thermoelectric Figure of Merit. *Phys. Rev. B: Condens. Matter Mater. Phys.* **1993**, *47* (19), 12727−12731.
(43) Kim, W.; Zide, J.; Gossard, A.; Klenov, D.; Stemmer, S.; Shakouri, A.; Majumdar, A. Thermal Conductivity Reduction and Thermoelectric Figure of Merit Increase by Embedding Nanoparticles in Crystalline Semiconductors. *Phys. Rev. Lett.* **2006**, *96* (4), 4.
(44) Hummers, W. S.; Offeman, R. E. Preparation of Graphitic Oxide. *J. Am. Chem. Soc.* **1958**, *80* (6), 1339−1339.
(45) Boffoue, O.; Jacquot, A.; Dauscher, A.; Lenoir, B.; Stolzer, M. Experimental Setup for the Measurement of the Electrical Resistivity and Thermopower of Thin Films and Bulk Materials. *Rev. Sci. Instrum.* **2005**, *76* (5), 053907−4.

DOI: 10.1021/acsami.6b09836
ACS Appl. Mater. Interfaces 2016, 8, 31617−31624